Pergamon

Atmospheric Environment Vol. 31, No. 14, pp. 2089–2105, 1997

PII: S1352-2310(96)00300-7
1352-2310/97 $17.00 + 0.00

THE VERTICAL CHEMICAL AND METEOROLOGICAL STRUCTURE OF THE BOUNDARY LAYER IN THE LOWER FRASER VALLEY DURING PACIFIC '93

K. L. HAYDEN, K. G. ANLAUF, R. M. HOFF, J. W. STRAPP, J. W. BOTTENHEIM, H. A. WIEBE, F. A. FROUDE and J. B. MARTIN
Atmospheric Environment Service, 4905 Dufferin Street, Downsview, Ont., Canada M3H 5T4

and

D. G. STEYN and I. G. McKENDRY
Atmospheric Science Programme, Department of Geography, University of British Columbia, Vancouver, British Columbia, Canada V6T 1Z2

(*First received* 12 *September* 1995 *and in final form* 23 *September* 1996. *Published May* 1997)

Abstract—Mixed layer depths were derived from potential temperature profiles from aircraft, high-altitude balloon sonde and tethersonde measurements taken during the Pacific '93 field study in the Lower Fraser Valley of southern British Columbia. In general, mixed layer depths derived from these different data sources were closely comparable. An airborne lidar was used to map aerosol depth throughout the valley. These lidar-derived aerosol depths compared well with the meteorologically derived mixed layer depths. During one notable ozone episode, mixed layer depths were low, and in the range 500–800 m. Measurements of chemical pollutants such as ozone and nitrogen oxides showed these to be generally well mixed below the top of the mixed layer during daytime. However, at times, layering within and above the inversion layer was observed. © 1997 Elsevier Science Ltd.

Key word index: Mixed layer depth, complex terrain, ozone episode, aircraft profiles, aerosol depth, ozonesonde, tethersonde, chemical species concentration.

1. INTRODUCTION

In the summer of 1993, an intensive field study was conducted in the Lower Fraser Valley (LFV) of coastal British Columbia to investigate the processes leading to frequent episodic ground-level ozone. Figure 1 shows a map of the LFV region with topographical contours. The LFV region covers complex terrain including both land and water surfaces, and is encompassed by mountain ranges to the north and from the south to the southeast. A significant pollution source in the valley is the city of Vancouver and its surrounding urban areas (vehicle and industrial emissions). In particular, there are several refineries in the Port Moody (PM) area along with a natural gas-fired power plant; in the southern part of the valley, there is another refinery complex on the coast, west of Bellingham (BA), U.S.A. Steyn *et al.* (this issue) provide an overview of the study including a history of ozone pollution in the valley, a description of the study region and measurement locations, measurements taken and highlights of results. A main objective of the field program was to collect data during an ozone episode to initialize and validate an urban airshed model of the photochemical and meteorological processes in the valley.

One of the most important atmospheric features affecting the concentration and dispersion of airborne pollutants is the meteorological structure of the boundary layer. Stull (1988) defines the boundary layer as "that part of the troposphere that is directly influenced by the presence of the earth's surface, and responds to surface forcings (frictional drag, evaporation and transpiration, heat transfer, pollutant emission and terrain induced flow modification) with a timescale of about an hour or less". Under convective conditions, the boundary layer is generally well-mixed with a temperature inversion capping further vertical mixing. Mean wind speed within this surface-based layer, and the layer's vertical extent (referred to as the mixed layer depth) are primary factors in determining ambient pollution concentration on regional scales. Steyn *et al.* (1990) show that mixed layer depths in the LFV have a dominant effect in determining the severity of ozone episodes. Therefore, to model such episodes, it is imperative to have measurements of mixed layer depth.

Mixed layer depths can be determined from profiles of temperature, moisture, and turbulent intensity, and more recently from acoustic sounder returns and lidar backscatter data. These methods generally detect slightly different boundary layer features, and therefore result in slightly different depths (Marsik *et al.*, 1995; Beyrich, 1994). In general, directly measured profiles of one or more meteorological variables (e.g. temperature from rawinsondes) appear to give the most accurate mixed layer depth estimates under the meteorological conditions studied (Marsik *et al.*, 1995).

Under conditions of light onshore winds and strong insolation, the mixed layer becomes a Thermal Internal Boundary Layer (TIBL) in the coastal zone (Gryning and Batchvarova, 1990). Over distances up to 100 km, this layer rises (in an approximately quadratic way) from its over-water depth (typically 50 to 100 m) to a continental depth (typically 1500 to 2000 m). Steyn and Oke (1982) and Gryning and Batchvarova (1996) investigated the spatial and temporal dependence of the TIBL in the LFV using data from a variety of instruments and two simple models of TIBL growth. These papers relied on data from only one site in the LFV. Cai and Steyn (1995), in a modelling study, diagnosed the TIBL depth from turbulent kinetic energy profiles calculated by a higher order closure scheme for boundary layer turbulence imbedded within a three-dimensional mesoscale meteorological model. The calculated depths compared well with measured values derived from two acoustic sounders and a tethered balloon flown within the LFV.

As part of the present LFV Oxidant Study, also termed Pacific '93, a Convair 580 aircraft was flown over the valley to characterize the structure of the boundary layer. Using aircraft-based lidar measurements, Hoff *et al.* (this issue) discuss aerosol sources and movement in the valley. In addition to these aircraft flights, ozonesondes were released at a site near the centre of the valley at Langley, and tethered ozonesondes were flown at an enhanced chemistry measurement site located at Harris Road (HR). Figure 1 shows the LFV region, with the locations of the various ground sites and locations of aircraft profiles discussed in this paper.

The purpose of this paper is to present an analysis of the vertical structure of the boundary layer and determine its effect on pollutant concentrations over the LFV during Pacific '93. Mixed layer depths as derived from measurements by sondes and aircraft-mounted meteorological, chemical and lidar instruments are discussed. This paper presents a data set on mixed layer depth, unique in terms of spatial and temporal coverage, for a region of complex coastline and topography.

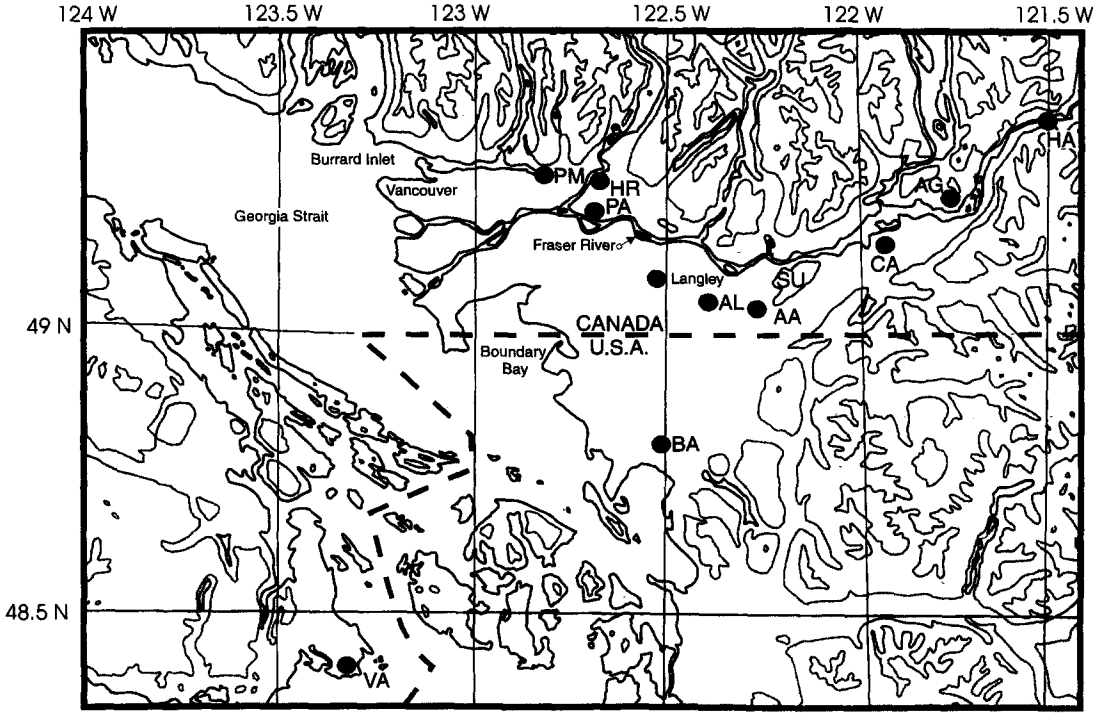

Fig. 1. Pacific '93 Field Study domain in the Lower Fraser Valley and surrounding Pacific region. The terrain contours are in intervals of 100, 500 and 1500 m. (AA = Abbotsford Airport, AL = Aldergrove, HA = Hope Airport, CA = Chilliwack Airport, PA = Pitt Meadows Airport, BA = Bellingham Airport, SU = south of Sumas, VA = Victoria Airport, AG = Aggasiz).

2. EXPERIMENTAL

2.1. *Aircraft measurements*

A Convair 580 aircraft, owned and operated by the National Research Council (NRC), completed sixteen flights throughout the study period of 15 July–12 August 1993, nine of which were during an "episode" between 31 July and 5 August. Most flights included both a high altitude portion (above 4000 m) in which a downward-pointing lidar measured aerosol backscatter over the valley, and a low level portion (usually below 1000 m) with horizontal transects and vertical profiles in the boundary layer. The former measurement was usually carried out first over a period of about 2 h, after which the aircraft descended to complete the latter boundary layer measurements, also about 2 h in duration.

The aircraft was outfitted by the Atmospheric Environment Service with meteorological instrumentation, a 1.064 μm Nd-Yag lidar and an air chemistry package consisting of continuous gas analyzers and batch sampling systems. NRC also maintained an aircraft instrumentation package for the measurement of pressure, temperature, altitude, position, winds and turbulence.

2.1.1. *Meteorological instrumentation.* Air temperature was measured using a standard de-iced Rosemount temperature probe mounted on the lower wing surface. Pressure was measured at a static pressure port located on the forward fuselage. An EG&G dewpoint hygrometer was also mounted on the forward fuselage. The altitude (height above surface) was calculated by taking the radar altimeter reading at the base of a profile, and then using the hydrostatic equation to integrate the "thickness" in meters at 1 s intervals to the top of the profile. Actual temperatures and pressures were used in these calculations. Water vapor mixing ratios and relative humidities were derived from the temperature, pressure and dewpoint measurements. Wind speeds and directions were calculated from ground speed measurements, derived from a Litton LTN 90-100 inertial reference unit and from the true air speed derived from the static pressure measured on the fuselage, and the total pressure measured on the starboard wing. The aircraft was equipped with a Rosemount (model 858) 5-hole pressure probe, from which aircraft angle of attack and sideslip were measured. These data were used to correct the true air speed data before calculating the winds by differencing the inertial and true air velocity components.

2.1.2. *Lidar instrumentation.* The downward pointing lidar determines the backscatter coefficient of the atmosphere at 1.064 μm including scattering from aerosols and Rayleigh scattering from air. A description of the lidar operation and procedures for extracting aerosol height information is given in Hoff *et al.* (this issue).

2.1.3. *Chemical instrumentation.* The chemical instrumentation on the Convair 580 aircraft is summarized in Table 1. The gas analyzers were calibrated during the field study with NIST (National Institute for Standards and Technology) reference transfer standards. Since each instrument had a significant time constant, the data were phase shifted to reduce lag errors affecting both vertical and horizontal definition. Although an attempt was made to measure NO_2 with a liquid-phase method, a final calibrated data set was not recoverable. Further details regarding aircraft measurements can be found in the Pacific '93 aircraft data report by Hayden *et al.* (1994).

2.2. *Surface measurements*

2.2.1. *Harris Road enhanced chemistry measurement site (HR).* This site was located on a dyke of the Pitt River about 40 km downwind of sources from Vancouver and about 10 km from the industrial center of Port Moody (PM). Steyn *et al.* (this issue) and Pottier *et al.* (1994) provide a further description of the HR site. In the following discussion, only those chemical measurements relevant to the aircraft will be considered. O_3 was measured continuously between 19 July and 6 August 1993 with a model 49 TECO UV photometric analyzer which was calibrated before, during and after the study. NO and NO_2 were measured by means of an Ecophysics Model CLD 770 analyzer and a PLC 760 photolytic converter. NO_y was measured with a modified commercial NO analyzer in combination with a heated gold converter and CO catalytic reduction. Calibrations of the nitrogen oxides instruments were made by means of a NIST NO cylinder and a carefully calibrated NO_2 permeation tube in conjunction with an air dilution system. Data were collected as 1-min averages.

2.2.2. *Greater Vancouver regional district (GVRD) sites.* The GVRD network comprises about 20 sites, measuring a variety of meteorological and chemical components on a continuous and routine basis. For the purpose of this paper, the following two sites are of particular importance: (1) Pitt Meadows airport GVRD site, located on a dyke within 500 m of the airport runway and about 7.8 km south of the HR surface site, and (2) Abbotsford GVRD site, located in town about 8.3 km northeast of Abbotsford airport. At these GVRD sites, O_3 was measured by TECO UV photometric analyzers, and NO and NO_x were measured by standard commercial chemiluminescence analyzers. These network sites report only 1-h averages (ending on the hour).

2.3. *Ozonesonde measurements*

Model ECC-5A ozonesondes were released at the Langley site usually four times per day during the episode period. Ozone concentrations and meteorological profile data including wind speed and direction, relative humidity, dewpoint and temperature were collected up to 12 km. Evans *et al.* (1994) provide a description of the ozonesonde. Surface sonde-derived ozone concentrations were found to be within 1–2 ppb of the Langley GVRD calibrated ozone measurements. Martin and Froude (1993) describe in detail the Langley site and ozonesonde measurements.

2.4. *Tethersonde measurements*

Vertical meteorological and ozone data were collected over the HR site by an Atmospheric Instrumentation

Table 1. Convair 580 aircraft chemical instrumentation

Chemical species	Instrument	Method	Time constant (s)	Detection limit (ppb)	Accuracy
O_3	TECO 49	UV photometric absorption	8	0.5	$\pm$ 0.5 ppb
NO	Ecophysics model CLD770	Chemiluminescence	20	0.1	< 5% for NO > 0.1 ppb
NO_y	Modified TECO model 42S	Chemiluminescence Au converter + CO gas	30	0.1	< 5% for NO_y > 1 ppb

Research Inc. Tethersonde (TS-3A-SPH) and an Ozonesonde (OZ-3A-T) beneath a $5\,m^3$ helium-filled tethered balloon. In this paper, references will be made only to meteorological information, while ozone measurements are discussed in a companion paper (McKendry *et al.*, this issue).

3. RESULTS AND DISCUSSION

3.1. *Sonde and aircraft-derived mixed layer depths*

Mixed layer depths were determined from the available aircraft and sonde meteorological profile data. Particular attention was given to examination of the potential temperature profiles, and, in the case of aircraft data, virtual potential temperatures were also considered. The virtual potential temperature is a desirable variable to consider in marine environments since it accommodates temperature variations caused by the presence of water vapor in the atmosphere (Stull, 1988). From the profiles, the mixed layer depth was defined as the height of the inversion closest to the surface where the potential temperature lapse rate was greater than $2\,K\,km^{-1}$ (with few exceptions, the difference between the top and bottom of the inversion layer was greater than 1 K and the vertical extent was more than 50 m). This lapse rate was adopted from the work of Garrett (1981) where it appeared to consistently discriminate between the turbulent mixing layer and more stable air above. Although this criterion is somewhat arbitrary, it provides a consistent, objective and quantitative method of analyzing potential temperature profiles for mixed layer depths.

More recently, Marsik *et al.* (1995) used two criteria for estimating mixed layer depths (also called mixing heights) during midsummer in the Atlanta region of the southern United States: firstly, the potential temperature lapse rate in the inversion layer must be $\geqslant 5\,K\,km^{-1}$ and secondly, the difference in potential temperatures between the top and base of the critical inversion layer be $\geqslant 2\,K$. The height (or depth) of the mixed layer was then taken at the altitude where the temperature was 2 K above the inversion base. The criterion selected for the Pacific '93 study was deemed sufficient given that little information on mixed layer depths in complex terrain was available. Furthermore, the validity of our simple criterion is ultimately tested by the measurements of pollutant concentrations within the derived mixed layer depth (see following Sections 3.3 and 3.4).

The presence of a well-defined temperature inversion usually fell within the $2\,K\,km^{-1}$ criterion which facilitated defining a mixed layer depth. However, in some cases, the inversion was more difficult to determine and required further analysis. Other meteorological profiles (e.g. changes in wind direction, wind speed and water vapour mixing ratio) usually revealed information to substantiate or reject mixing depths chosen from potential temperature profiles. Table 2 provides a complete, detailed summary of mixed layer depths derived from meteorological profiles by aircraft, ozonesonde (at Langley) and tethersonde (at Harris Road), as well as from lidar profiles for the period 19 July–6 August 1993. Some general observations are evident from Table 2. The midday mixed layer depths from 1–6 August at Abbotsford airport (AA) and Pitt Meadows airport (PA) were similar to the central valley sonde site at Langley. During the ozone episode period, 3–6 August, the aircraft descents at the shoreline Bellingham airport (BA) site revealed substantially lower mixed layer depths than elsewhere because this coastal location is generally covered by the shallow marine boundary layer. At the two sites further inland, Chilliwack airport (CA) and Hope airport (HA), the mixed layer depths (300–800 m) as derived from aircraft measurements were lower than those measured in the center of the valley (800–1100 m; between 23 July and 1 August 1993).

Figure 2 shows a more extensive comparison between the Langley sonde-derived mixed layer depths and those derived by aircraft profiles at Abbotsford airport (AA) where most of the descents/ascents were made. From the figure, the diurnal maxima in mixed layer depths are readily evident. The aircraft-derived mixed layer depths compare reasonably with those from the Langley sondes, although it is about 22 km to the west of Abbotsford. Because of strong convective activity, mixing could extend above the derived mixed layer depth into the inversion layer. Hence, on Fig. 2, for each mixed layer depth, the vertical extent of the inversion layer (or entrainment zone) is indicated so as to provide an upper limit to these derived mixed layer depths. For the 1–5 August period, low mixed layer depths during midday, in the range 500–800 m (cf. typical summertime continental mixed layer depths of 1.5–2 km), undoubtedly aided the formation of relatively high ozone during this episode period.

To aid in the comparison of mixing heights derived from different platforms and locations, Figs 3a–c show correlation diagrams comparing midmorning to late afternoon mixed layer depths as derived from the two sondes and the aircraft-mounted lidar with those derived from the aircraft meteorological probes. The lidar-derived mixed layer depths and their derivation are discussed in detail in the following section. As evident in Fig 3a, the Langley sonde results show some agreement with those from the aircraft meteorological probes at Abbotsford Airport (AA), both sites being situated well within the valley. In general, Langley mixed layer depths are lower than those derived by aircraft profiles at AA, which is located further in the valley. Although the comparison in Fig. 3b has fewer data points, it appears that the tethersonde-derived mixed layer depths are also low with respect to those from the aircraft. A possible reason for this may be the effect of the local complex terrain. The boundary layer at the tethersonde location at Harris Road (HR) may be significantly modified by the close proximity of the mountains that define the

Table 2. Summary of mixed layer depths (in meters above ground level (m, agl)) derived from aircraft, ozonesonde, tethersonde and LIDAR profiles for July 19–August 6, 1993

	Time (PST)	Aircraft profile	Langley ozonesonde	Harris Rd. Tethersonde	LIDAR
		m, agl	m, agl	m, agl	m, agl (Time, PST)
July					
19	12:13	625 AA			
	14:51	640 AA			
23	12:44	600 AA			759 (13:31)
	14:00		738		
	15:05	800 AL			
26	7:00		0		
	10:39	810 AA			
	13:00		993		
	13:33	800 HA			837 (13:20)
	15:11			600	
	15:35			500	
27	5:00		0		
	7:24	250 AA			
	9:14	350 HA			288 (09:04)
	9:39	350 CA			
	10:08	400 AA			
	17:43	1050 AL			
31	5:00		218		
	14:00		1018		
	16:00		818		
	16:02	1220 AA			
Aug.					
1	4:00		0		
	6:40			0	
	7:07			0	
	7:37			100	
	7:41	300 AA			
	8:09			140	
	9:42			500	
	10:00		568		
	10:12			440	
	10:21	400 HA			332 (10:11)
	10:41	300 CA			
	11:00			660	
	11:29			540	
	11:52	825 PA			
	12:44	680 AA			
	13:05			620	
	13:26			640	
	14:00		743		
	14:34	850 AA			
	16:00		593		
	16:40	730 HA			
	16:55			700	
	17:18			200	
	18:04			0	
	18:26	0 AA			
	19:00		0		
2	4:00		0		
	7:15			0	
	7:40			0	
	7:55	0 AA			
	8:33			80	
	9:04			220	
	10:00		243		
	10:49	280 AA			
	12:41			300	
	13:00		793		
	13:02			560	
	16:00		643		
3	4:00		0		
	9:09	300 AA			200 (09:32)
	11:25	375 HA			

Table 2. (*Continued*)

	Time (PST)	Aircraft profile	Langley ozonesonde	Harris Rd. Tethersonde	LIDAR
		m, agl	m, agl	m, agl	m, agl (Time, PST)
	11:35			350	
	11:52			300	
	12:46	400 PA			
	12:52			400	
	13:00		518		
	13:09			400	
	13:28	200 BA			
	13:50	400 CA			
	16:00		293		
	18:32	440 CA			
4	4:00		0		
	9:17			80	
	9:40			130	
	10:00		308		
	10:48			330	
	11:43			510	
	11:53	420 AA			
	12:07			520	
	12:59	775 PA			
	13:00		418		
	13:22	410 BA			
	13:39	600 AA			
	15:47	1100 SU			1100 (15:24)
	16:00		368		
	16:18	460 AA			
5	4:00		0		
	5:42	0 AA			
	8:19			0	
	9:03	200 HA			185 (08:51)
	9:26	300 CA			
	9:50	400 PA			
	10:00		568		
	10:03			300	
	10:20			430	
	10:39			420	
	10:54	100 VA			
	12:23			520	
	12:48	100 VA			
	12:55			620	
	13:00		718		
	13:11			700	
	14:48	750 AG			
	15:09			580	
	15:31			600	
	15:48	825 PA			
	16:00		443		
	16:14	180 AA			
	17:26			640	
	17:40			440	
	18:05			0	
	18:20			0	
6	4:00		0		
	6:21	150 AA			
	7:20			140	
	8:00			300	
	9:51			480	
	10:00		418		
	10:06			310	
	10:13	150 VA			
	11:22			460	
	11:40			500	
	12:20			560	
	12:37			580	
	13:05			600	
	13:09	150 VA			
	13:26			600	
	13:59			630	

Table 2. (*Continued*)

Time (PST)	Aircraft profile	Langley ozonesonde	Harris Rd. Tethersonde	LIDAR
	m, agl	m, agl	m, agl	m, agl (Time, PST)
14:19			500	
14:50			600	
15:12			620	
15:15	440 BA			
15:37			620	
15:56			680	
16:00		518		
16:07	680 PA			
17:08	300 AA			
17:26			500	
17:37			400	
18:00			400	
18:15			0	

(AA = Abbotsford Airport, AL = Aldergrove, HA = Hope Airport, CA = Chilliwack Airport, PA = Pitt Meadows Airport, BA = Bellingham Airport, SU = south of Sumas, VA = Victoria Airport, AG = Aggasiz).

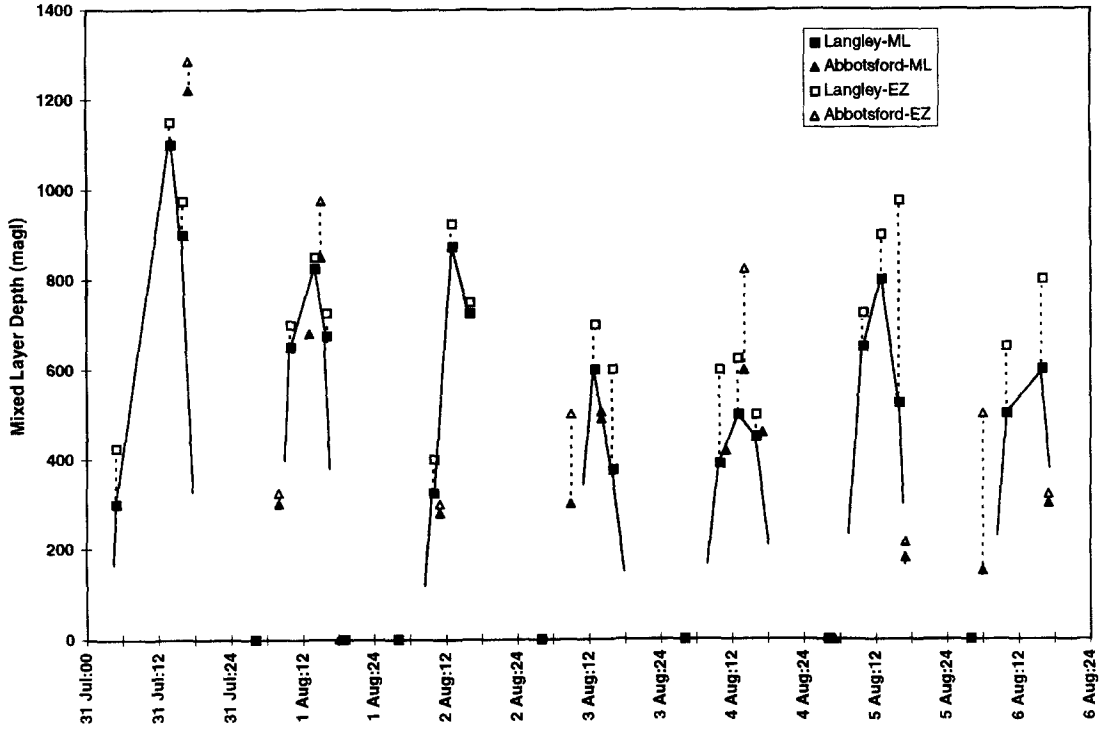

Fig. 2. Mixed layer depths (ML) and entrainment zones (EZ) from Abbotsford airport aircraft profiles and Langley ozonesondes.

northern limit of the valley and the mouth of the Pitt Lake canyon. The aircraft profiles were, however, made over Pitt Meadows Airport (PA), about 8 km to the south, further in the valley and less influenced by the valley edge topography. As might be expected, the mixed layer depths at Harris Road (HR) were lower than those at Langley, even further in the valley, because the boundary layer would have deepened further inland. The most consistent agreement was found between the aircraft lidar and meteorologically derived mixed layer depths (see Fig. 3c). Maybe this should not be surprising because both measurements were from the same aircraft measurement platform, and, hence, differences in geographical location and measurement times were minimized (the lidar data was averaged over a distance of about 2.5 km, except for one case at 4 km).

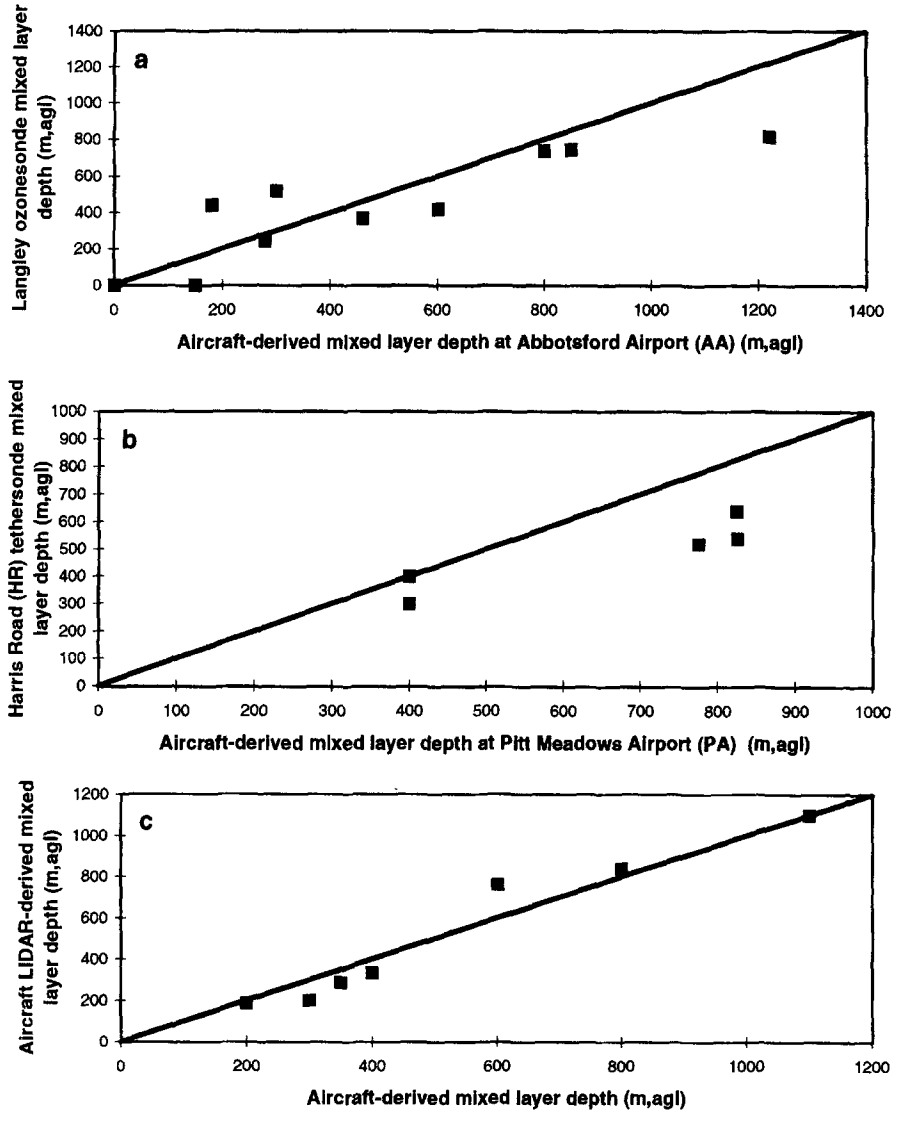

Fig. 3. (a) Langley ozonesonde mixed layer depths vs aircraft-derived mixed layer depths at Abbotsford Airport (AA); m, agl = meters above ground level. (b) Harris Road (HR) tethersonde mixed layer depths vs aircraft-derived mixed layer depths at Pitt Meadows Airport (PA); m, agl = meters above ground level. (c) Aircraft lidar-derived mixed layer depths vs aircraft-derived mixed layer depths; m, agl = meters above ground level.

For the most part, the mixed layer depths as derived from the four different platforms show reasonable agreement. This supports the validity of the meteorological and lidar criteria used to derive these mixed layer depths.

3.2. *Lidar-derived mixed layer depths*

Mixed layer depths can also be inferred from lidar measurements if the production of aerosols below the inversion is sufficient to generate a gradient in the aerosol backscatter ratio (Hoff *et al.*, 1994). This procedure defines the position of the largest negative derivative, $-\mathrm{d}B/\mathrm{d}z$ (where B is the lidar backscatter ratio) as the height of the mixing layer. Further details for this procedure can be found in Hoff *et al.* (1994). Because of localized variability in the lidar backscattering from individual plumes and irregularities, it was found that horizontal averaging of 10 s of aircraft travel (approximately 1.2 km) and vertical smoothing of 5 points (60 m) using a running mean filter improved the mixed layer height retrievals. After gridding these heights in latitude and longitude, the gridded data were smoothed with a weighted 3-point averaging filter, giving an effective spatial resolution of about 2 km. Since the algorithm can detect layers aloft, 1200 m, asl (meters above sea level) was used as a constraint on the retrieval for all flights but one. The exception was flight P310 on July 31 when convective

activity formed cumulus cell tops up to 1800 m. Another confounding factor was the widely varying topography over the valley and the algorithm often reported heights of greater than one km over mountainous terrain. Upon examining the profiles it was clear that the true mixed layer height was only a few hundred meters, at most, on these hillsides. Therefore, to remove this topographical artifact, the "aerosol depth" was defined as the derived mixed layer height minus the local terrain height. Within the valley, the aerosol depths were nearly identical to the mixed layer heights because the valley is largely flat and near sea level. If surface mixing is strong and no overlying aerosol layers occur, the aerosol depth and the mixed layer depth (as previously discussed) should be identical. However, processes have been identified in this valley (elevated plumes from sources and recirculation from orographic flows; see McKendry *et al.*, this issue) leading to elevated layers that produce stronger signals than the surface-generated aerosols, especially in morning hours. Contours of lidar-derived aerosol depths were determined by gridding the derivative data into $0.1 \times 0.1°$ cells. In Figs 4a–e, the top panel shows a three-dimensional view of the aerosol (or mixed layer) depth over the coordinate range (49.0°N, −123.5°W to 49.5°N, −121.5°W) which contains the Canadian portion of the LFV. The vertical range of the axis in these graphs is 1000 m. The lower panel shows a simplified map of the LFV with the oceanic shoreline, the Fraser River and four

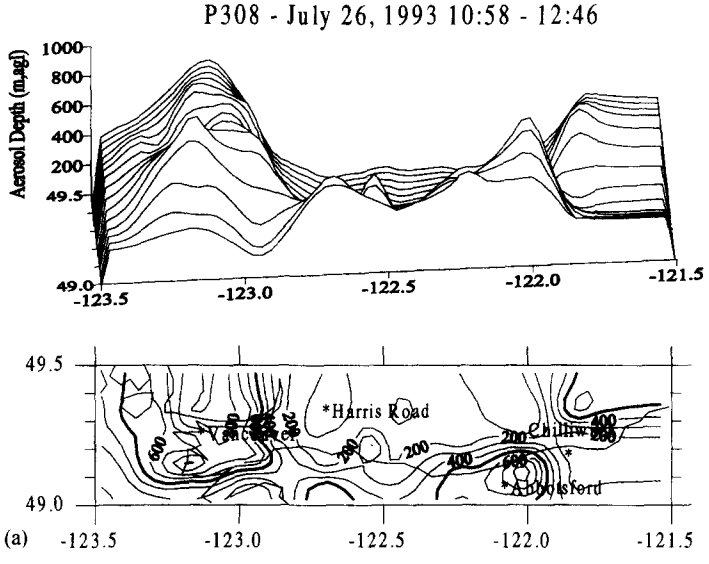

Fig. 4a. Lidar-derived aerosol depths over the Lower Fraser Valley for 26 July 1993; m, agl = meters above ground level.

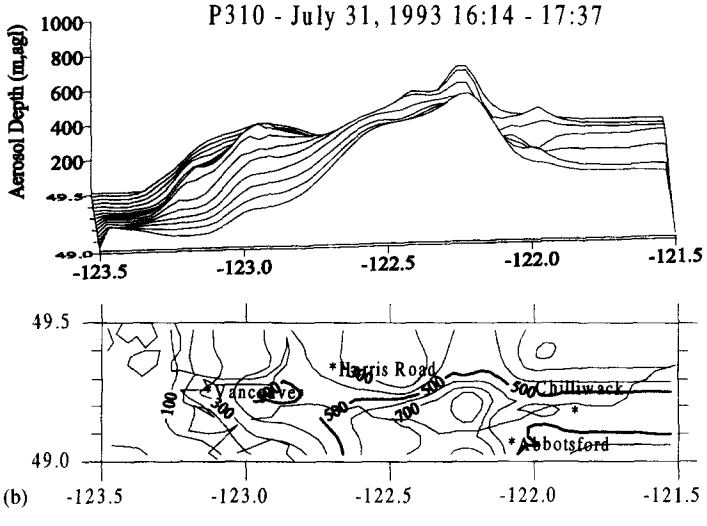

Fig. 4b. Lidar-derived aerosol depths over the Lower Fraser Valley for 31 July 1993; m, agl = meters above ground level.

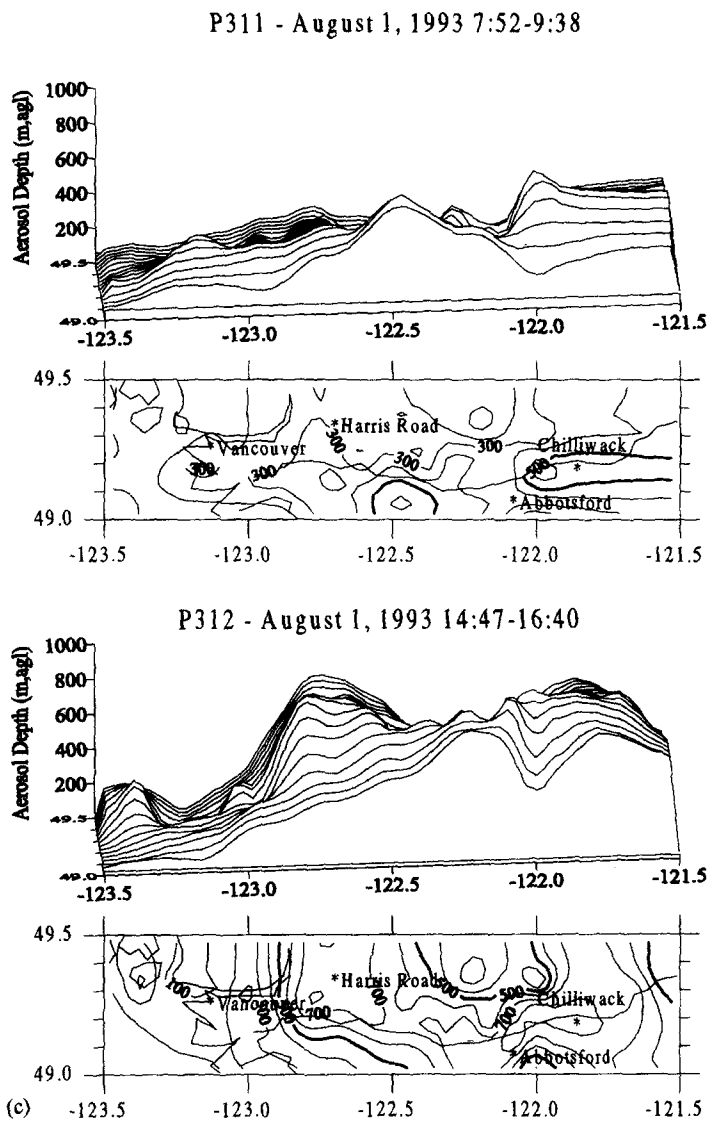

Fig. 4c. Lidar-derived aerosol depths over the Lower Fraser Valley for (i) the morning of 1 August 1993, (ii) the afternoon of 1 August 1993; m, agl = meters above ground level.

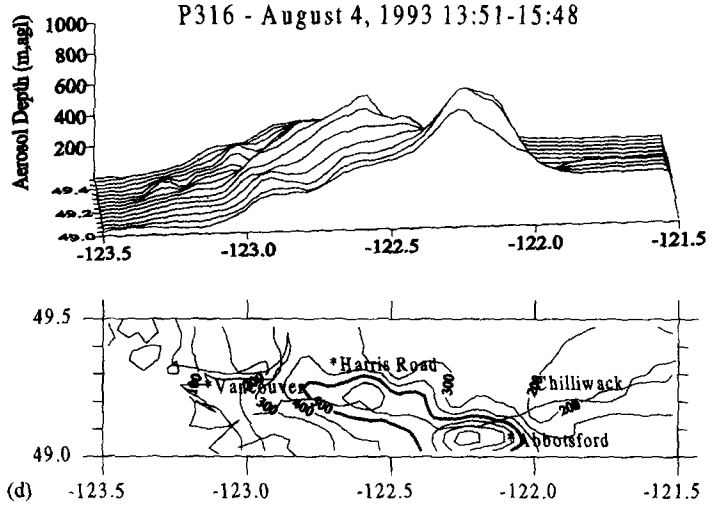

Fig. 4d. Lidar-derived aerosol depths over the Lower Fraser Valley for 4 August 1993; m, agl = meters above ground level.

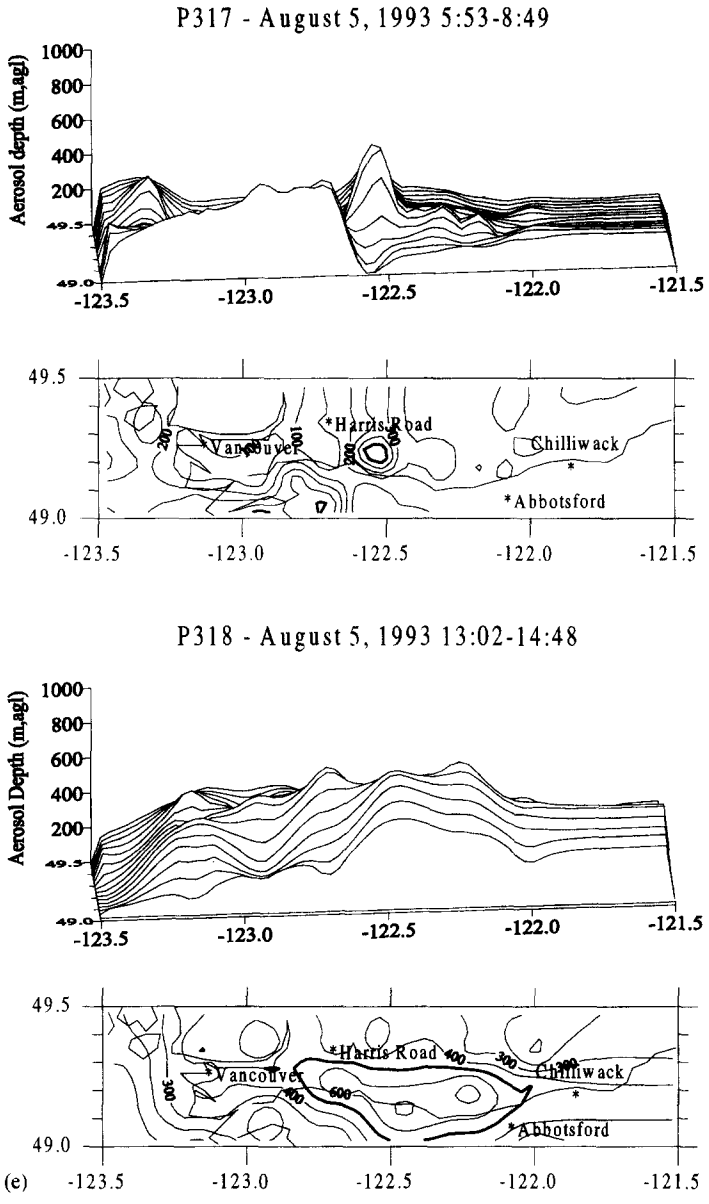

Fig. 4e. Lidar-derived aerosol depths over the Lower Fraser Valley for (i) the morning of 5 August 1993, (ii) the afternoon of 5 August 1993; m, agl = meters above ground level.

locations including Vancouver, Harris Road, Abbotsford and Chilliwack. The contours of aerosol depth (in meters) are superimposed, with the 500 m contour (and 1000 m contours, where appropriate) emboldened.

Figure 4a shows the lidar-derived aerosol layer depth from the late morning flight on 26 July (Flight P308). There was a large increase in the general 200 m boundary layer depth over the urban area of Vancouver and in the eastern part of the valley near Abbotsford. The former bulge is due to the heat island of the city of Vancouver. The latter boundary layer increase appears to be greatest at the U.S./Canada border and is due to the aerosols produced by the refineries near Cherry Point in Washington state.

Figure 4b shows the lidar-derived aerosol depth from Flight P310 on 31 July. The boundary layer grows monotonically from the shoreline inland at the north side of the valley. On the southern side, however, the aerosol in the vicinity of Abbotsford shows a greatly increased depth. This haze mass appeared to be residual material left from the previous day and was noted not to be associated with the Vancouver plume at this time of the morning.

Figure 4c(i) gives the aerosol depth from the lidar cross-sections on the morning of 1 August. The aerosol depth was generally 300 m throughout the entire land portion of the LFV and below 100 m over the Georgia Strait. This compares well with an aircraft observation which showed a mixed layer depth of

300 m at Abbotsford Airport at 0741 PST (see Table 2). The 500 m bulge in the boundary layer at − 122.5°W appears to be lofting of the refinery plume from the shoreline near Bellingham.

Figure 4c(ii) shows the afternoon flight on 1 August. The afternoon mixed layer depths, 700–800 m at their highest point, were significantly greater than on the previous morning. Likewise, the aircraft also showed an increase in mixed layer depth on 1 August from the morning to the afternoon flight (see Table 2). Specifically, at Abbotsford airport it increased from 300 to 850 m and at Hope airport it increased from 400 to 730 m. The gradient from the shoreline was quite steep in the vicinity of Vancouver and could be interpreted as the morning heat island plume from the city being advected eastward in the early afternoon sea breeze.

For the early morning flight of the lidar on 2 August, there was essentially no heating in the valley and the aerosol depth was 100–200 m throughout the valley. On 2 and 3 August, the morning surface inversions were stronger than on 31 July and 1 August (Pottier, 1995). In particular, the lidar over Abbotsford at 0955 PST indicated an aerosol depth (mixed layer depth) of 250 m and the aircraft over the same location at 1049 PST showed a strong inversion at 280 m.

The morning flight of 3 August (P314) showed low aerosol depths through much of the LFV with only a minor rise to about 300 m near Chilliwack. An aircraft descent at Abbotsford airport at 0909 PST also measured a mixed layer depth of 300 m.

Figure 4d depicts flight P316 on 4 August which was taken during the early afternoon. The contours of the aerosol depth reveal a deep boundary layer extending from the Port Moody area to Abbotsford. The highest mixed layer depth determined by the lidar was 800 m near Abbotsford. The aerosol depth over the Georgia Strait was well under 100 m and grew monotonically from the shoreline inland. The mixed layer depth as derived from the aircraft temperature profile (steep inversion) was between 600–825 m at Abbotsford airport at 1339 PST and lower at 410 m at Bellingham airport at 1322 PST.

On 5 August, two flights were made. In the first, at 0553–0849 PST, the lidar determined that the highest aerosol tops were right at 49.0°N near the shoreline. This is clearly due to the refinery plumes originating from the Bellingham area. Outside of a single high feature in the mid-LFV, the boundary layer was typically 100–200 m deep throughout the entire valley (see Fig. 4e(i)). There is no other evidence to validate this 500 m aerosol depth in the center of the valley. Aircraft descents were not made until some time later in the morning, between 0930 and 1000 PST at Chilliwack airport and Pitt Meadows airport; by this time, the mixed layer depths at these locations had grown to 300 and 400 m, respectively.

During the afternoon flight of 5 August, 1302–1448 PST (see Fig. 4e(ii)), the boundary layer had grown to about 600–700 m in the mid-LFV and was about 300 m near the shoreline and in the eastern end of the valley. The aircraft profiles at Agassiz (about 15 km east of Chilliwack, 1448 PST) and Pitt Meadows airport (1548 PST) showed the mixed layer depth to be 750–825 m; this would indicate that the boundary or mixed layer was still growing after the lidar run.

The lidar results have shown that the boundary layer structure, when corrected for underlying topography, is driven primarily by three factors: local heating (including buoyancy effects from the urban heat island of Vancouver city), stability of the overlying inversion, and IBL growth from the shoreland eastward into that inversion. Venkatram (1977) showed that the IBL growth is given by

$$h(x) = \frac{u_*}{u_m}\left[\frac{2(T_l - T_w)x}{\gamma(1-2F)}\right]^{1/2}$$

where u_* is the friction velocity, u_m is the IBL mean wind speed, T_l is the maximum land temperature, T_w is the water temperature, γ is the potential temperature lapse rate, and F is the ratio of heat flux entrained at the top of the IBL compared to the surface heat flux and is often approximated by 1/7 (Tennekes, 1973). From a preliminary look at the episode period, 4 and 5 August (Fig. 4d and e(ii)) were chosen for comparison to the IBL model. One of these cases illustrates close agreement to theory, whereas the other shows complicating features. For this analysis, u_* was chosen as 0.3 m s^{-1}. T_l, u_m and γ were derived from the Langley ozone soundings at 0500, 1000 and 1300 PST and from the Abbotsford surface observations at 1400 PST.

Figure 5 shows the evolution of the temperature profile at the Langley upper air site for the first five days of August. For each day, the thin solid line represents the 0500 PST profile and the bold line is the 1300 or 1400 PST profile. The profiles do not show the classical IBL evolution described by Venkatram (1977), but there is clear definition of the mid-afternoon inversion jump. The early morning inversion structure during the period of 31 July to 5 August showed strong positive lapse rates of up to 0.0026 K m^{-1} right off the surface with γ in the range of 0.0046–0.0096 K m^{-1} above 500–800 m altitude. Using the lapse rates from the region above the midday inversion overpredicts IBL growth. Using early morning lapse rates in the surface inversion (the lapse rate into which the IBL must grow) gives better agreement with Venkatram's prediction. The estimated lapse rates within the afternoon entrainment zone are shown as a dotted line on Fig. 5. It is these lapse rates that we have used in the IBL prediction below.

Figure 6 shows the result for 4 August for a transect with the lidar which ran in a westerly direction down the middle of the LFV. Since the mixing height contours previously shown have been smoothed, it was felt that a direct comparison with one transect would

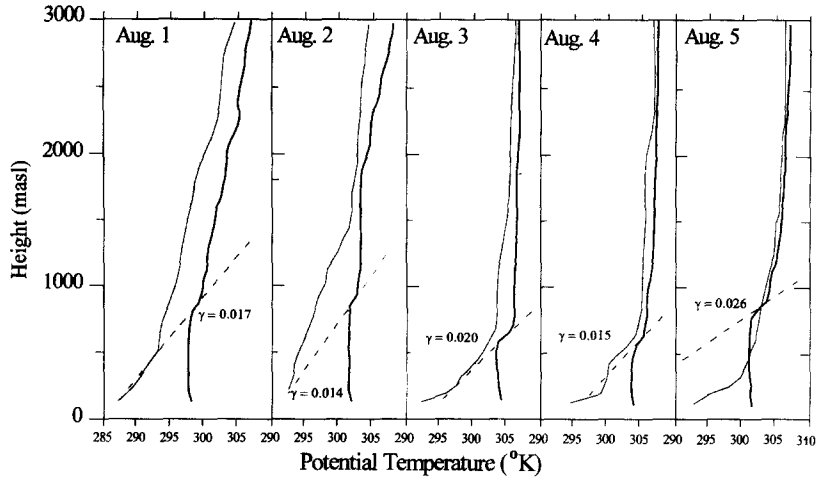

Fig. 5. Morning (0500 PST, solid line) and afternoon (1300 or 1400 PST, bold line) potential temperature profiles from the Langley upper air site for 1–5 August. The dotted line shows the potential temperature lapse rate within the entrainment zone; m, asl = meters above sea level.

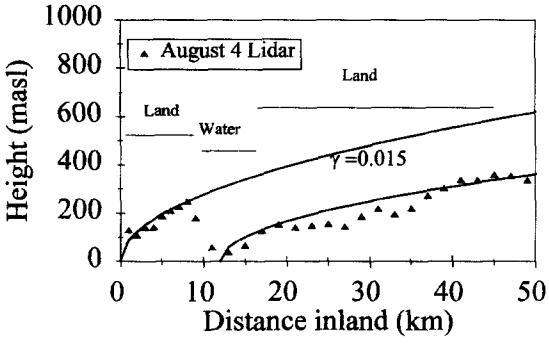

Fig. 6. IBL growth from the shoreline in a west to east direction just north of the Canada–U.S. border for the afternoon of 4 August. The lidar measurements (triangles) are compared to the IBL model (solid curve). Two modelled IBL curves are shown due to a readjustment in the boundary layer as the wind passed over Point Roberts (9 km stretch of land) to Boundary Bay (5 km stretch of water) and then into the LFV (land); m, asl = meters above sea level.

be best for this comparison with the model above. The transect shown (T2W on 4 August at 15:17–15:31 PST) is complicated by the fact that it passed over Point Roberts, a peninsula extending southward to the west of Boundary Bay. The transect covered a 9 km section of land, an approximate 5 km stretch of water or tidelands, and then passed into the Fraser Valley; this flight track was just north and parallel to the Canada—U.S. border. The predicted IBL growth is shown from the 0 km position using an air temperature of 29°C, a water temperature of 18°C, $\mu_m = 4.9\,m\,s^{-1}$ and $\gamma = 0.0015\,K\,m^{-1}$. Near the shore the growth is correct and then the IBL adjusts to Boundary Bay. We assumed that Boundary Bay was 6°C warmer than waters of the Georgia Strait and readjusted the IBL model to restart at a position 12 km inland. From that location eastward, the growth is close to the simple model of Venkatram.

On 5 August, the flow in the afternoon was SSW at $6.1\,m\,s^{-1}$, with an air temperature of 27.7°C, water temperature of 20°C and $\gamma = 0.0026\,K\,m^{-1}$. These factors made a much shallower IBL. Figure 7 shows a south–north transect on 5 August coming in off Georgia Strait and passing directly over the city of Vancouver and Burrard Inlet to the north of the city. Since the wind was not normal to either the shoreline or the flight track, an adjustment for inland fetch was made by dividing the aircraft inland distance by $1/\cos(23°)$, which was the angle between the mean wind and the flight track and also approximated the additional fetch from the western end of the city. The growth is again reasonable using the simple IBL model with a few notable exceptions. At 10 km from the shore, an industrial plume gave rise to additional heating. At 28 km, the city of Vancouver also gave rise to an additional 100–200 m of boundary layer height. Over Burrard Inlet, at 38 km, cold water collapsed the IBL which rose again on the north side of Burrard Inlet.

One conclusion which can be drawn is that the IBL growth near the shoreline can be modelled with reasonable accuracy for the middle of the nonurbanized part of the valley. However, when the boundary layer grows above 500 m (at distances far inland or where there are significant buoyant sources, such as the urban heat island of Vancouver), the less stable layer above 500 m comes into play and convection is less restrained. This explained many of the large height "bubbles" which are seen in the lidar mixing height contours. In these cases, the heating penetrates the strongest early morning lapse rate and extends into the less stable air above, generally with another inversion at the ~ 1–1.5 km level which is tied to the orography at the north of the valley. Clearly, with

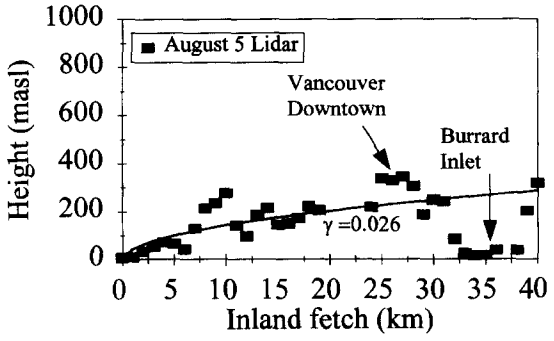

Fig. 7. IBL growth as a function of inland fetch (km) in a south-north transection (L11N) of the lidar on August 15. The lidar measurements (squares) are compared to the IBL model (solid curve). Extra heating is seen from an industrial plume at 10 km and Vancouver downtown at 27 km, while at 35 km the cool surface of Burrard Inlet collapses the boundary layer; m, asl = meters above sea level.

orographic effects and urban heat sources a more sophisticated model than simple IBL models will be needed to understand the mixing height growth through the valley.

3.3. *Chemical mixing in the boundary layer*

The degree of chemical mixing within the boundary layer is reflected in the vertical structure of chemical constituents. To explore the extent of vertical mixing, aircraft profiles of trace gas concentrations including O_3, NO_y and NO, were examined. During midday, a photostationary state is a good approximation and a chemical relationship exists where the ambient ozone is proportional to the ratio of NO_2/NO. The vertical O_3 profiles were used as a qualitative indicator of a well-mixed boundary layer. However, it is important to examine the parallel NO and NO_y (includes NO_2, NO, HNO_3 and PAN) profiles because local ground-level emissions of NO will rapidly titrate (decrease) ozone with a corresponding increase in NO_2.

Figures 8a–c show profiles for three days of the study, 3, 4 and 6 August, which illustrate some typical chemical vertical structures during the episode period. To facilitate the comparison of profiles at several locations, the y-axis has been normalized to the meteorologically derived mixed layer depth for the particular profile and the chemical species concentration is plotted on the x-axis. O_3 profiles were examined for the presence of a surface-based, well-mixed layer with a distinct change in concentration near the temperature inversion. (Ground-level concentrations from nearby surface sites were not included in the aircraft profile figures because of time resolution and horizontal heterogeneity factors discussed in the following section.)

For the two days, 3 and 4 August (see Figs 8a and b), the chemical species concentration dropped markedly in the region of the meteorologically determined mixed layer depth (using the potential temperature as the chief criterion as discussed in the Section 3.1), and for both days, ozone was well mixed within the mixing layer. For the nitrogen oxides, at times, the time resolution of the analyzers and/or the low concentrations obscured any change in concentration within or near the top of the mixed layer depth. However, for the several cases where the nitrogen oxides were sufficiently high, their uniformity within the mixed layer along with the sharp decrease at the inversion altitude is readily evident (e.g. PA and AA profiles). These observations provide key qualitative evidence to substantiate the common modelling assumption that pollutants are well-mixed below the inversion during active convective conditions as present during the early August episode period. Also, this shows that daytime surface chemistry measurements can be representative of the total mixing layer.

On 6 August, the flow in the Lower Fraser Valley was clean Pacific air from the southwest and concentrations were generally low. At the Pitt Meadows Airport (PA) location, an ozone layer aloft was observed (see Fig. 8c) with the ozone maximum in the entrainment zone. (The nitric oxide was uniform below the inversion although at very low concentration.) On this day, the ozone bulge above the inversion seemed to be the result of strong wind sheer near the inversion and recirculation of pollutants into this upper layer from other parts of the valley. McKendry *et al.* (this issue) discuss this case in more detail and conclude that pollutants overlying the inversion can be important in entrainment processes resulting in chemical concentration increases in the boundary layer. Nevertheless, on this day, the ozone was well mixed at Pitt Meadows Airport (PA) throughout the mixing layer below the temperature inversion. At Bellingham Airport (BA), a marine location, there was no such obvious layer aloft, and the ozone decreased below 500 m, possibly because of underlying marine boundary layer effects.

3.4. *Aircraft versus surface measurements*

In order to determine how representative ground-based measurements are of the boundary layer, some surface-based chemical concentrations were compared to those taken by the aircraft. Measurements of O_3, NO and NO_y were available from the aircraft and the HR surface site. Data from the Pitt Meadows airport GVRD site included O_3, NO and NO_x, while only O_3 was used from the Abbotsford downtown GVRD site. Aircraft descents were made over Pitt Meadows airport (PA), some 8 km south of Harris Road (HR), and Abbottsford airport (AA) by means of a landing approach (thereafter, the aircraft ascended and resumed its normal flight track). The instantaneous values at the base of the descent from the aircraft continuous analyzers were compared to 1-min averages from the HR enhanced chemistry site or 1-h averages from the GVRD network sites. Since the aircraft did not penetrate the boundary layer on all descents, only those profiles where measurements were taken well within this layer were included in the comparison.

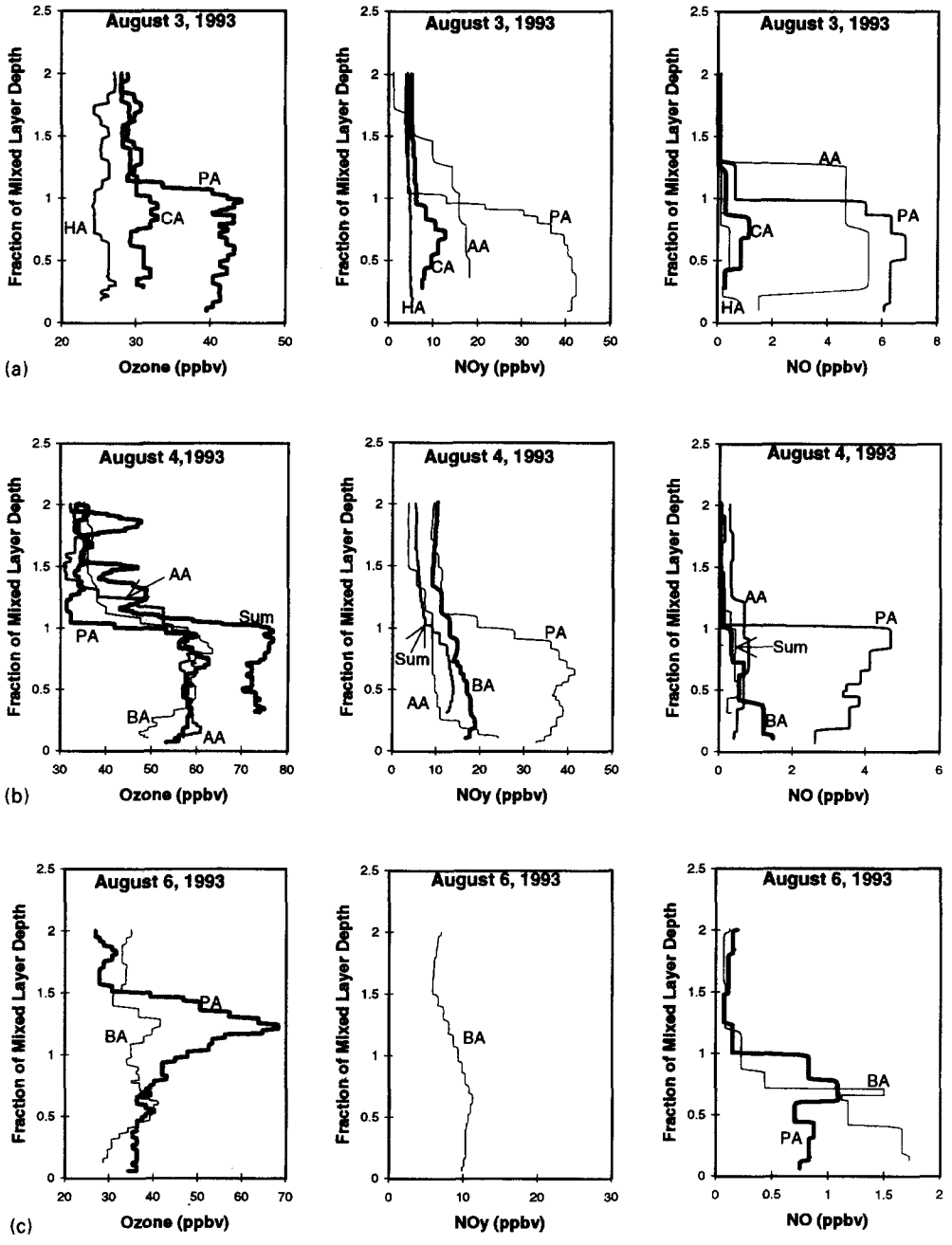

Fig. 8. (a) Chemical concentrations within the mixing layer on 3 August, 1993. (PA = Pitt Meadows airport; 1246 PST, HA = Hope airport; 1125 PST, CA = Chilliwack airport; 1350 PST, AA = Abbotsford airport; 0909 PST); (b) chemical concentrations within the mixing layer on 4 August, 1993. (PA = Pitt Meadows airport; 1259 PST, AA = Abbotsford airport; 1339 PST, BA = Bellingham airport; 1322 PST, Sum = south of Sumas mountain; 1547 PST); (c) chemical concentrations within the mixing layer on 6 August, 1993. (BA = Bellingham airport; 1515 PST, PA = Pitt Meadows airport; 1607 PST).

Some horizontal heterogeneity in ozone and nitrogen oxides between the HR and PA locations were found. Figures 9a–c show a comparison of aircraft concentrations with those at the HR and GVRD surface sites. Because most PA aircraft descents were carried out close to the hour, the two-hourly averages for the PA GVRD site encompassing the time of the aircraft descent are indicated as (+) symbols with a solid line joining the two points. The linear regression equation and r^2 for the aircraft (over PA) vs HR surface data are indicated on each graph. Figure 9a shows that the aircraft-measured O_3 over PA was lower by 5–15 ppb than that at the HR surface site. For the nitrogen oxides, NO is shown to be quite

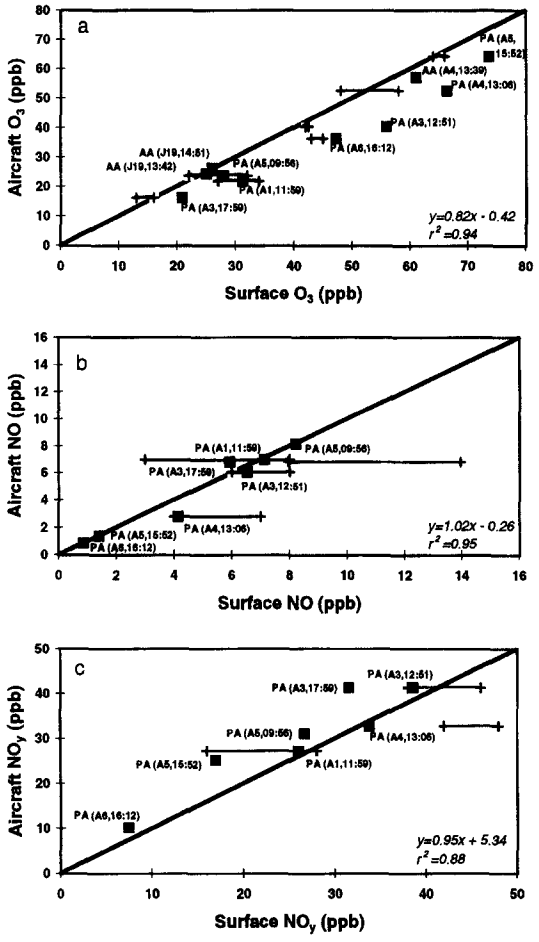

Fig. 9a–c. Aircraft comparisons with surface sites (PA = Pitt Meadows airport, AA = Abbotsford airport, e.g. J23 = July 23, A5 = August 5, 09:56 = time of aircraft measurement in PST). The filled squares are the 1-min Harris Road or 1-h Abbotsford GVRD surface concentrations compared with the instantaneous aircraft descent concentrations over PA or over AA respectively. The horizontal lines, terminated by (+) symbols, indicate the range of the two hourly concentrations at the PA GVRD surface site spanning the time of the aircraft descent over PA.

close to the 1:1 line in Fig. 9b, whereas Fig. 9c shows that the aircraft-measured NO_y over PA was higher by up to 10 ppb than at HR. In and immediately downwind of urban areas, NO_y consists mostly of NO and NO_2; therefore, the lower O_3 at PA, relative to the HR site, could be attributed to recent titration by fresh NO emissions from surface sources in the local area (e.g. vehicular traffic). Not surprisingly, close agreement exists when ozone as measured at the PA GVRD site is compared to the corresponding aircraft descents over the adjacent airport. Similarly, agreement is close at Abbotsford.

The limited comparisons shown in the above three figures do show that low altitude aircraft measurements agree reasonably with those taken at the surface, especially when the time resolution of the concentration data is sufficiently short. However, in situations of horizontal heterogeneity as is common downwind of urban areas, care must be exercised when comparing aircraft descents at locations different from surface sites.

4. CONCLUSIONS

Observations from high altitude balloon sondes, aircraft profiles and tethered balloon sondes were presented to illustrate spatial and temporal variations in mixed layer depth in a region of complex coastline and topography. Using a criterion of 2 K km^{-1} gradient in the potential temperature profile to define the top of the mixed layer, mixed layer depths determined from the three different observing platforms were found to be similar. When differences were apparent between aircraft, balloon sonde and tethersonde, they could usually be attributed to the fact that observations were not co-located within the valley and therefore differences reflected real spatial variations in mixed layer depth. Mixed layer depths were also determined from an aircraft-mounted downward-looking lidar. Generally, these calculated aerosol depths compared well with aircraft profile estimates of mixed layer depth. However, under some conditions, particularly in early morning or when layers of pollutants or clouds were evident aloft, estimates of mixed layer depths could be misleading if not examined carefully. These results are in agreement with those of Marsik *et al.* (1995).

On the basis of temperature profiles, daytime mixed layer depths were observed to vary significantly from day to day during the period of observations. On days in which boundary layer ozone concentrations were relatively high (particularly 1–5 August), mixed layer depths were in the range 500–800 m. These characteristically shallow mixed layers can be attributed to a combination of synoptic scale subsidence and the nearshore thermal internal boundary layer structure. Profiles of several chemical species showed that, generally, concentrations of pollutants are well-mixed below the top of the mixed layer during daytime. This provides confirmation for a widely held assumption in photochemical modelling. However, the results do indicate that on some occasions, polluted layers may exist at or immediately above the top of the mixed layer. Such layers are frequently observed in regions of complex coastal terrain (McKendry *et al.*, this issue) and may contribute significantly to boundary layer concentrations through vertical mixing processes. These observations suggest that models based on the simple mixing of pollutants from surface emission sources through a convective mixed layer should take into account the possibility of downward mixing from layers aloft and recirculation of pollutants on timescales longer than a day.

The use of the downward-looking aircraft-mounted lidar to determine the depth of aerosol layers (surface-based) permitted the mapping of aerosol depth for the

entire LFV. Together with the profile data, these observations show that mixed layer depths within the LFV are highly variable, both spatially, and from day to day. Accurate simulations of the local air quality problem will therefore be heavily dependent on the ability of mesoscale meteorological models to capture such variability.

In summary, the results described herein are in broad agreement with studies of mixed layer depth elsewhere in complex coastal terrain. In addition to providing a valuable comparison of different methods of estimating mixed layer depth, this extensive data set highlights the complex spatial and temporal variation in mixed layer depth in a coastal valley. Such complexity provides an important challenge for modellers.

Acknowledgements—We wish to express our gratitude to the project staff of the Institute for Aerospace Research of NRC for their contributions in outfitting the aircraft, its operation and in data collection, M. Watt for technical assistance on the aircraft measurements program, K. Sung for his diligence in aircraft data abstraction, J. Pottier for helpful discussions on the prevailing meteorological conditions during the study, B. Thomson for coordinating the expert assistance of the AES Pacific Region, M. Wasey for the aircraft instrument installation and operation, and Environment Canada for providing funding for this project. This paper is contribution number 96-07 of the Canadian Institute for Research in Atmospheric Chemistry.

REFERENCES

Beyrich F. (1994) Intercomparison of different methods for mixed layer depth estimation in the convective boundary layer from sodar data. In *Proc. 7th Int. Symp. on Acoustic Remote Sensing and Associated Techniques of the Atmosphere and Ocean* (edited by Neff W. D.), Boulder, Colorado, 3–7 October 1994, pp. 2-19–2-25.

Cai X. and Steyn D. G. (1995) Mesoscale meteorological modelling study of the Lower Fraser Valley, B.C., Canada, from July 17 to 20, 1985. Contract report to Environment Canada. August 1995. (Also as The University of British Columbia, Department of Geography, Occasional Paper No. 40).

Evans C., Martin B., Froude F. and Thomson R. B. (1994) Ozone and meteorological profiles in the Lower Fraser Valley of British Columbia. Air and Waste Management Annual General Meeting, Proc. November 1993. Pacific Northwest International Section. (Also as Internal Report, Report # PAES-93-7, to the Pacific Region, Atmospheric Issues and Services Branch, Atmospheric Environment Service, Pacific Region, Suite 700, 1200 W. 73rd Avenue, Vancouver, B.C.).

Garrett A. J. (1981) Comparison of observed mixed-layer depths to model estimates using observed temperatures and winds, and MOS forecasts. *J. appl. Met.* **20,** 1277–1283.

Gryning S. E. and Batchvarova E. (1990) Analytical model for the growth of the coastal internal boundary layer durign onshore flow. *Q. J. R. Met. Soc.* **116,** 187–203.

Gryning S. E. and Batchvarova E. (1996) Modeling the internal boundary layer height over the Vancouver area. *Ninth Joint Conf. on the Applications of Air Pollution Meteorology*, American Meteorological Society and Air and Waste Management Association, Baltimore, 28 January–2 February 1996.

Hayden K. L., Anlauf K. G., Hoff R. M. and Strapp J. W. (1994) Pacific '93 Lower Fraser Valley Oxidants Study: aircraft data report, July 1994. Atmospheric Environment Service, 4905 Dufferin Street, Downsview, Ontario, Canada M3H 5T4.

Hoff R. M., Harwood M. and Sheppard A. (1994) Pacific '93 — aircraft lidar project: preliminary results. Atmospheric Environment Service, 4905 Dufferin Street, Downsview, Ontario, Canada M3H 5T4.

Hoff R. M., Harwood M., Sheppard A., Froude F. A., Martin J. B. and Strapp J. W. (this issue) Use of airborne lidar to determine aerosol sources and movement in the Lower Fraser Valley (LFV), B.C. *Atmospheric Environment*, **31,** 2123–2134.

Marsik F. J., Fisher K. W., McDonald T. D. and Samson P. J. (1995) Comparison of methods for estimating mixed layer depth used during the 1992 Atlanta Field Intensive. *J. Appl. Met.* **34,** 1802–1814.

Martin J. B. and Froude F. A. (1993) Data report: Lower Fraser Valley Oxidants Study (Pacific '93) Langley B.C. Sonde Release Site July 13–August 12 1993, Atmospheric Environment Service, 4905 Dufferin Street, Downsview, Ontario, Canada M3H 5T4.

McKendry I. G., Steyn D. G., Lundgren J., Hoff R. M., Strapp J. W., Anlauf K. G., Froude F. A., Martin J. B., Banta R. M. and Oliver L. D. Elevated layers and vertical down-mixing over the Lower Fraser Valley, B.C. *Atmospheric Environment*, **31,** 2135–2146.

Pottier J. L. (1995) An investigation of upper level, boundary layer and surface meteorology in the Lower Fraser Valley during Pacific '93 (August 1–6, 1993) Atmospheric Issues and Services Branch, atmospheric Environment Service, Pacific Region, Suite 700, 1200 W. 73rd Avenue, Vancouver, B.C.

Pottier J., Thomson R. B., Bottenheim J. and Steyn D. (1994) Pacific '93 meteorology records July 15–August 12, 1993 Part of Lower Fraser Valley Oxidants Study. Atmospheric Issues and Services Branch, Atmospheric Environment Service, Pacific Region, Suite 700, 1200 W. 73rd Avenue, Vancouver, B. C.

Steyn D. G. and Oke T. R. (1982) The depth of the daytime mixed layer layer at two coastal sites: a model and its validation. *Boundary-Layer Met.* **24,** 161–180.

Steyn D. G., Roberge A. C. and Jackson C. (1990) Anatomy of an extended air pollution episode in British Columbia's Lower Fraser Valley. Prepared for BC Ministry of Environment.

Steyn D. G., Bottenheim J. W. and Thomson R. B. (1996) Overview of tropospheric ozone in the Lower Fraser Valley, and the Pacific '93 field study. *Atmospheric Environment*, **31,** 2025–2035.

Stull R. B. (1988) *An Introduction to Boundary Layer Meteorology*. Kluwer, Norwell, MA.

Tennekes H. (1973) A model for the dynamics of the inversion above the convective boundary layer. *J. atmos. Sci.* **30,** 558–567.

Venkatram A. (1977) A model of internal boundary-layer development. *Boundary-Layer Met.* **11,** 419–437.